The Thesis Committee for Roberto Amilcar Hernandez
certifies that this is the approved version of the following thesis:

Monte-Carlo Simulations of a Comptonization model for the Photospheric Process

APPROVED BY

SUPERVISING COMMITTEE:

Duane Dicus, Supervisor

Pawan Kumar

Monte-Carlo Simulations of a Comptonization model for the Photospheric Process

by

Roberto Amilcar Hernandez, B.S.

THESIS

Presented to the Faculty of the Graduate School of

The University of Texas at Austin

in Partial Fulfillment

of the Requirements

for the Degree of

MASTER OF ARTS

THE UNIVERSITY OF TEXAS AT AUSTIN

August 2015

Dedicated to Daniela, Federico, Patricia, Alejandro, and all of those who supported me throughout this journey.

E quindi uscimmo a riveder le stelle.

Dante Alighieri
Divina Commedia

Monte-Carlo Simulations of a Comptonization model for the Photospheric Process

Roberto Amilcar Hernandez, M.A.
The University of Texas at Austin, 2015

Supervisor: Duane Dicus

This thesis presents the results of numerical simulations of an Inverse-Compton scattering model for the photospheric process. We use a Monte-Carlo method to simulate the processing and broadening of Planckian radiation below the Thomson photosphere of hot relativistic outflows. A new numerical code was developed and allowed us to explore a completely new region of the parameter space, in particular a higher and more realistic photon-to-electron ratio. The results may be relevant to the prompt emission of Gamma-ray Bursts (GRBs), Tidal Disruption Events (TDEs), and other high-energy transients where optically thick outflows are present.

Table of Contents

List of Figures

Chapter 1

Introduction

1.1 Overview

High-energy transients are some of the most fascinating events in the known universe. Their short duration and almost unbelievable energy release makes us associate them with some of the most exotic and enigmatic objects, like black-holes, neutron stars, and stellar deaths. The study of high-energy transients presents many challenges however, from their aforementioned short duration (as short as tens of milliseconds), to the need of specialized space-based instruments to observe them. More than forty years after the discovery of these phenomena, there are still many questions left to answer and, even though substantial progress has been made in many of these, our physical understanding in some areas is basic at best. It should be mentioned, however, that despite the difficulties associated with the study of these objects, we probably live in a golden era for the advance and exploration of this field: the amount and quality of panchromatic data, combined with advances in numerical and computational methods make the solution of these enigmas more feasible than ever.

In a very broad and general sense, it is possible to decompose the study and understanding of high-energy transients into separate, though interconnected, problems:

- What is the progenitor of these events? What is the central engine powering the event?
- What is the structure and composition of the (sub)relativistic outflow?
- What is the energy dissipation mechanism? What is the particle acceleration mechanism?
- What is the radiation mechanism? Where is most of the energy being radiated?
- What are the properties of the transient nearby environment?

Perhaps the greatest difficulty is that some of these questions are not only related but their solution is degenerate. This means that in most cases only educated guesses can be made about parts of the solution, making it nearly impossible to distinguish between alternate models.

The problem of a radiation mechanism in a specific set of conditions (what could be called a system), nonetheless, is one where progress can be made: different models (systems) have different spectral and temporal signatures that can be exclusive and serve as what is known as a "smoking gun". There are terrific books that cover the different processes in great detail and rigor such as Rybicki & Lightman (1986), Longair (2011), and Melia (2009); but for our purposes, it suffices to distinguish between two types of systems:

1. Optically thick systems: Any kind of system where the radiation is produced at a Thomson optical depth $\tau \gg 1$, and that combined with the right set of conditions will produce a Planckian spectrum.

2. Optically thin systems: In these systems radiation can escape without being significantly modified by the environment, yielding different spectral and temporal signatures than optically thick systems. The observed spectrum is most of the times of a non-thermal nature, e.g., a power-law.

Both types of system have their own strengths and limitations in describing the observed spectra of transients, and there are several instances where there is confidence in the collective properties of the system responsible for the observed emission, e.g., synchrotron radiation from an external forward shock in an optically thin outflow being responsible for the late-time afterglow of Gamma Ray Bursts (GRBs) (Panaitescu & Kumar, 2001, 2002; Yost et al., 2003).

One outstanding problem in particular is the radiative process responsible for the prompt emission of GRBs. A description of the observational characteristics of the prompt can be found in Kouveliotou et al. (1993); Fishman & Meegan (1995), but the most difficult ones to explain are its spectral features. The prompt emission can be described by an empirical function called the Band function (Band et al., 1993) (see Briggs et al. (1999) for an example of a case where the spectrum can be well fitted by this function). The Band function consists of two power-law segments joined at a peak energy with an average value of $\nu_p \approx 200 - 300$ keV (Preece et al., 2000). The spectral indices, in the f_ν sense, are usually $\alpha+1$ and $\beta+1$ for the low and high energy component, respectively, i.e., $f_\nu \propto \nu^{\alpha+1}$ for $\nu \leq \nu_p$ and $f_\nu \propto \nu^{\beta+1}$ for $\nu \geq \nu_p$.

The non-thermal nature of the Band function makes it an ideal candidate to be described by a radiation mechanism in an optically thin system. Different models can explain the observed distribution of values of β (Daigne

et al., 2011; Zhang & Yan, 2011), but the progress for α has been less fortunate. The issue lies in the fact that the average value of the low-energy index is $\langle\alpha\rangle \approx -1$ (Preece et al., 2000), and it is believed that in the case of synchrotron radiation the system would be in the fast-cooling regime, which predicts a photon index of $-3/2$ (Sari et al., 1998). Moreover, a significant fraction of bursts show values of alpha greater than $-2/3$ (Goldstein et al., 2012), thus crossing the so called "synchrotron line of death" (Preece et al., 1998). This poses an even bigger problem for the optically thin synchrotron mechanism.

It does then seem worthwhile to consider mechanisms in optically thick environments, despite the obvious point that the observed radiation is of a non-thermal nature. However, there are processes that can modify and broaden the initially quasi-thermal spectrum and potentially yield the required spectrum. They will be discussed in the next section.

1.2 The Photospheric Model

As mentioned in Section 1.1, radiation mechanisms in an optically thick system tend to produce quasi-thermal spectra since the radiation is produced at high optical depths, thermalizing quickly and wiping out any signatures of the initial production mechanism. Nonetheless, there are ways to process or modify the initial spectrum so that the observed one is non-thermal. Two types of effects are geometrical effects (Pe'er & Ryde, 2011; Lundman et al., 2013; Ito et al., 2014; Bégué & Iyyani, 2014), where factors like jet-structure, jet-geometry, and equal arrival time hypersurfaces tend to broaden and flatten the spectrum; and Comptonization effects, where the photons are Compton scattered by hot electrons multiple times and thus their energy is modified

(Ghisellini & Celotti, 1999; Mészáros & Rees, 2000; Beloborodov, 2010; Lazzati et al., 2013). In this work, we will focus on the latter.

The analytical expressions for the power spectrum for a single scattering between a photon and hot (or warm) electron are well known (see Rybicki & Lightman, 1986, pp. 195-208). However, unless the radiation is produced very close to the Thomson photosphere the photons will experience multiple scatterings before escaping the outflow. This problem is much more complex and there are three different approaches to solve it (Vereshchagin, 2014):

1. Solving a system of Boltzmann equations.
2. Solving the Kompaneets equation.
3. Performing Monte-Carlo (MC) simulations.

Let us briefly discuss each method:

1. System of Boltzmann equations: The most general and self-consistent approach to the problem is to solve a system of Boltzmann equations, one for the number density of electrons per unit Lorentz factor $n_e(\gamma_e, t)$ and the other for the number density of photons per unit energy per unit volume $n_\gamma(\epsilon, t)$.

   Analytical solutions to this system of integro-differential equations exist only for the simplest cases and the numerical solution of this system involves complex finite difference methods limited by grid size and resolution issues.

2. Kompaneets equation: The Kompaneets equation (Kompaneets, 1956) is a special case of the Boltzmann equation under the Fokker-Planck approximation, where the electrons are considered to be non-relativistic and the energy transfer from electron to photon per scattering is small.

Just like the Boltzmann equation, the Kompaneets equation can be solved analytically only for simple special cases. Even with good numerical solutions, it fails to capture the physics in the case of hot (relativistic) electrons with temperatures $k_B T_e > 511$ keV.

3. Monte-Carlo simulations: This method is completely independent from the previous two. In this statistical method, each photon is followed in from its initial injection position while it experiences numerous collisions before it eventually escapes the outflow. It has the advantage that it can deal with all sorts of electron temperatures and to easily model the Compton scattering. On the other hand, the main disadvantages are that it has to be implemented in an iterative or serial scheme, and the number of photons required to get good statistics means a large memory utilization and long computational runtimes. An increase in the computational resources available for use helps to alleviate the latter.

Considering the previous work done on approaches 1. and 2., combined with the increased availability of computational resources and the latest and most efficient compilers, we decided to follow approach 3. The details of our implementation are explained in the next chapter, along with a presentation of our main results.

Chapter 2

Monte-Carlo Simulations of an IC model of the Photospheric Process

2.1 Overview

The standard framework for the Photospheric process is that of the 'fireball' model (Goodman, 1986; Paczynski, 1986). We intend not to provide a rigorous and detailed presentation of this model, but only one that suffices to understand the results presented here (for a more in-depth presentation, see the reviews of Piran (2004); Kumar & Zhang (2015)). The 'fireball' is speculated to form at a small radius (comparable to the size of the progenitor, which is believed to be a stellar mass black hole or a milli-second magnetar) with a temperature $T \sim 10^{10}$ K; loaded with pairs, baryons, neutrinos, and photons.

As the 'fireball' expands adiabatically, it accelerates and the initial energy in radiation is converted to bulk motion of the outflow (i.e., protons get accelerated). After this, a fraction of the energy is converted back to random motion by a dissipation mechanism (either in a single or multiple events), and is radiated away by some mechanism either below or above the photosphere.

On the other hand, as the 'fireball' expands its Thomson optical depth decreases until the outflow becomes optically thin. But before that, the photons have experienced multiple Compton scattering events with hot electrons

heated by one or many dissipation events. These Compton and Inverse-Compton scatterings will modify the energy of the photons and thus the assumed initial Planckian spectrum.

The number of scattering events depends on the Thomson optical depth of the outflow, τ, which is given by (Kumar & Zhang, 2015, eq. (128)):

$$\tau \approx \frac{L\sigma_T}{8\pi r m_p c^3 \Gamma^3} \tag{2.1}$$

where L is the isotropically equivalent luminosity, m_p is the proton mass, r is the distance measured in the lab or center-of-explosion frame, and Γ is the bulk Lorentz factor of the outflow. The photospheric radius $R_{\rm ph}$ is defined as the radius where $\tau = 1$, that is,

$$R_{\rm ph} \approx \frac{L\sigma_T}{8\pi m_p c^3 \Gamma^3} \approx (5.5 \times 10^{12}\,{\rm cm}) L_{52} \Gamma_2^{-3} \tag{2.2}$$

On the last step we have used the fiduciary values to normalize the equation, as well as the commonly used notation $Q_n \equiv Q/10^n$. Now, one of the most important quantities in this model is the photon to electron ratio (see Santana et al., 2015, eq. (2))

$$\frac{N_\gamma}{N_e} = 10^6 \left(\frac{\eta}{1-\eta}\right) \Gamma_3 E_{\rm pk,6} \tag{2.3}$$

Here $E_{\rm pk}$ is the peak energy of the radiated spectrum measured in eV, and $\eta = E_\gamma/(E_\gamma + E_j)$ represents the jet radiative efficiency – E_γ and E_j being the radiated and jet kinetic energy, respectively. We see then that, for an efficiency of $\eta \sim 0.1$ and typical GRB values, a ratio of $\sim 10^5$ is necessary in order to physically reproduce the conditions of the outflow. Previous works

have focused on photon to electron ratios in the range of $10^1 - 10^4$ (Lazzati & Begelman, 2010; Chhotray & Lazzati, 2015), but never in the more realistic ratio of 10^5. This fact, combined with the availability of the computational resources required to run such ratios motivated us to develop a new code capable of handling this previously unexplored region of the parameter space.

The details of the code, as well as the implementation algorithm, are explained in detail in Santana et al. (2015). The conceptual idea is the following: photons and electrons are placed at an initial radius with their momentum (energy), initial position, and direction of motion sampled according to well defined functions , e.g., Planck function for the photons energy, Maxwell-Boltzmann function for the electrons momentum, etc.

After both types of particles have been initialized, the code begins the propagation of the photons by performing one scattering at a time. The distance each photon travels in the jet-comoving frame before encountering a randomly selected electron is sampled from a distribution that takes into account the mean-free path of the photon at its current position. Once the encounter takes place, we calculate the cross-section for the interaction between photon and electron and draw a random number to determine if the scattering takes place or not. After this, we update the necessary quantities of both photon and electron depending on whether the scattering took place or not.

We repeat this process until a chosen fraction of the photons propagate above the photospheric radius $R_{\rm ph}$, thus escaping the outflow. It is worthwhile mentioning that our code takes into account several key physical factors, such as:

- A priority queue system that guarantees that photons are scattered in a physically consistent sequence.
- Klein-Nishina effects in the interaction cross-section.
- Both Compton and Inverse-Compton scattering, allowing energy transfer from photons to electrons and vice versa.
- Keeping track of the electrons' energy and momentum, and not just that of the photons'.
- Relativistic kinematics for the outflow and their effect on the expected average number of scatterings for a given optical depth.
- Adiabatic cooling of both photons and electrons as the outflow expands.

As listed in Santana et al. (2015), the simulation parameters and their typical values are:

- Γ – The bulk Lorentz factor of the outflow. We used $\Gamma = 300$ based on the inferred average value of Γ for GRBs (Molinari et al., 2007; Xue, R.-R. et al., 2009; Liang et al., 2010). A few tests were run with different values of Γ as well.
- $L_{\rm iso}$ – The isotropic equivalent kinetic luminosity of the outflow. We use a value of $L_{\rm iso} = 10^{52}$ erg/s, in agreement with observations (Liang et al., 2007; Wanderman & Piran, 2010). A few tests were run with different values of $L_{\rm iso}$ as well.
- N_e – The number of electrons in a simulation. We initially considered $N_e = 10^3$ as the minimum value based on Lazzati & Begelman (2010),

and decided to investigate if indeed 10^3 electrons were enough. In Santana et al. (2015) we perform a comparison with results using $N_e = 10^4$ and the same photon-to-electron ratio, and find an excellent agreement. We will thus use $N_e = 10^3$ as our typical value.

- Electron Distribution Type. We considered three types of distribution: mono-energetic where all the electrons have the same Lorentz factor γ_e. Maxwell-Boltzmann (MB) where we define the comoving electron temperature T'_e as $k_B T'_e = (\gamma_{\rm elec}^{\rm AD} - 1)(\gamma_e - 1) m_e c^2$, where $\gamma_{\rm elec}^{\rm AD} = (4\gamma_e + 1)/3\gamma_e$ is the adiabatic index of the electrons; we have chosen this expression to make a smooth transition between the relativistic and non-relativistic definitions of temperature[1]. Power-law (PL) satisfying $dN_e/d\gamma_e \propto \gamma_e^{-p}$, with the power-law extending from $\gamma_{e,1}$ to $\gamma_{e,2}$.

- N_γ – The number of photons in a simulation. Based on the N_γ/N_e ratio given by eq. (2.3) and the previously mentioned value of N_e, our typical value is then equal to 10^8.

- T'_γ – This is the temperature in the jet comoving frame to which the photons are initialized. Different temperatures are explored, including $k_B T'_\gamma = 300$ eV, 100 eV, and 30 eV.

- $\tau_{\rm initial}$ – The optical depth corresponding to the distance from the central engine where the photons are initialized. We consider different values in the range $2 \leq \tau_{\rm initial} \leq 16$.

[1]Recall that $\langle {\rm KE} \rangle = \frac{3}{2} k_B T$ for a non-relativistic ideal gas and $\langle {\rm KE} \rangle = 3 k_B T$ for a relativistic one (Pathria & Beale, 2011).

- $\tau_{\rm photosphere}$ – The optical depth corresponding to the location of the photosphere after which it is unlikely for a photon to undergo any additional scatterings. At this radius, we collect the photons to produce the observed spectrum. We set $\tau_{\rm photosphere} = 1$.

- $N_{\rm reheat}$ – The number of additional dissipation events. We explore a range of $N_{\rm reheat} = 5 - 1000$

- Adiabatic Cooling – Whether Adiabatic Cooling (AC) is on/off during the simulation.

- $N_{\rm collect}$ – The number of photons collected for the output spectrum. Our typical fraction is 1/3, but other fractions were tested.

- Constant-Energy (CE) scheme – Whether the total energy available for dissipation is kept constant or not. In the first case a fixed amount of energy is distributed between all dissipation events ($N_{\rm reheat} + 1$), which means the dissipated energy per event will depend on $N_{\rm reheat}$. In the second case we dissipate the same amount of energy in each reheating event as that of the initial event. This scheme was only considered for mono-energetic and MB distributions, and the total amount of energy is set by $\gamma_{e,\rm total}$ instead of γ_e.

- Spread fraction – The fraction of the interval $[\tau_{\rm initial} \geq \tau \geq \tau_{\rm photosphere}]$ over which the reheating events take place. A fraction of one corresponds to the whole $[\tau_{\rm initial}, \tau_{\rm photosphere}]$ interval, a fraction of 1/2 would correspond to $[\tau_{\rm initial}, (\tau_{\rm initial} - \tau_{\rm photosphere})/2]$, and so on.

2.2 Code tests

Before running simulations with previously unexplored parameters, it was necessary to run several tests to check the validity of the code.

Figure 2.1 shows a comparison of results from our code with the ones from the code developed by Lazzati & Begelman (2010). We chose Fig. 4 of that paper in order to perform a comparison at different optical depths. The simulation parameters were set to match those of Lazzati & Begelman (2010). Note that, besides small deviations at the very high end, there is excellent agreement between the results of both codes. Furthermore, a Kolmogorov-Smirnov (KS) test reveals that the probability that both numerical results are sampled from the same underlying distribution is at least ≥ 0.985 for each case, further validating the previously stated agreement between codes. This increases our confidence that our code is producing physically sound results.

In addition to compare our results with previous codes, it is also necessary to justify why some parameters were not explored and their values kept constant.

- Γ: The LF of the outflow has two effects: to increase the energy of photons in the observer frame via Doppler boosting, and to change the expected average number of scatterings a photon experiences before escaping the outflow for a given optical depth τ. The first one has no impact in the shape of the spectrum, only on the position of the peak. The second one does affect the shape since for a relativistic outflow the expected average number of scatterings changes from $\tau^2_{\rm initial}$ to $2\tau_{\rm initial}$ (Bégué et al., 2013; Vereshchagin, 2014); however, the number is the same as long as the outflow is relativistic and independent on the actual

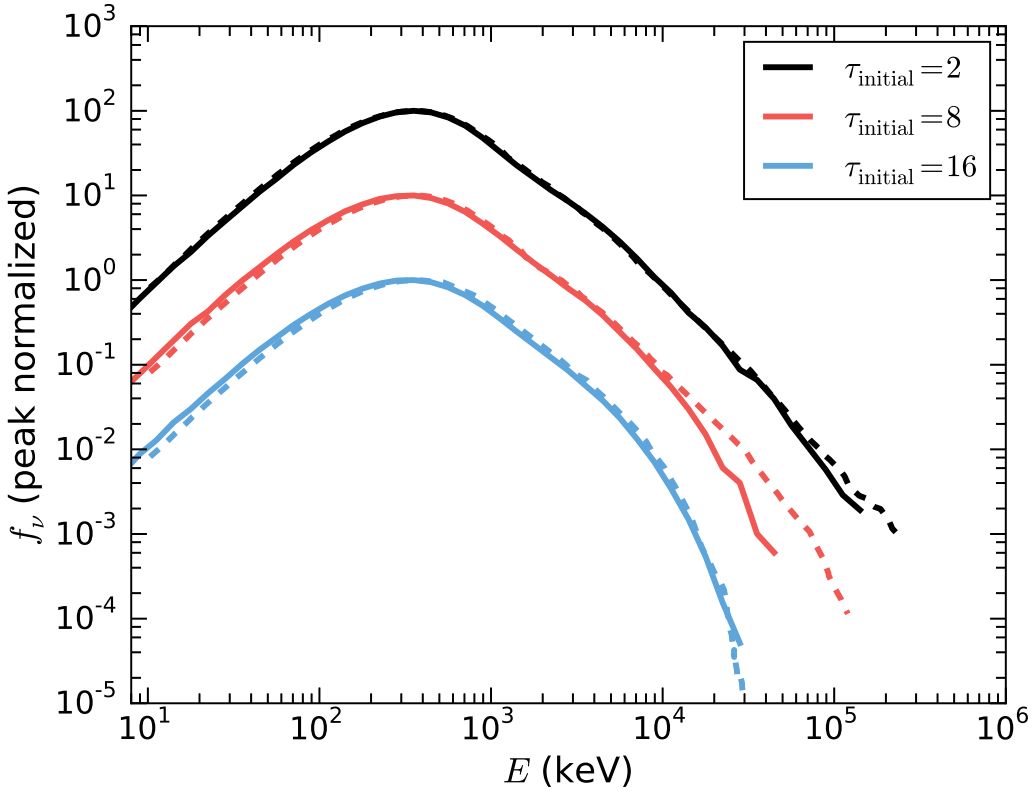

Figure 2.1: Comparison of the results of our MC code (solid lines) to those presented in Fig. 4 of Lazzati & Begelman (2010) (dashed lines). The simulation parameters are chosen to match those of Lazzati & Begelman (2010): mono-energetic electrons with $\gamma_e = 2$, $\Gamma = 1000$, $k_B T'_\gamma = 120$ eV, $N_\gamma = 3 \times 10^6$, $N_e = 10^3$, and no AC.

value of Γ (Bégué et al., 2013; Vereshchagin, 2014). A few simulations were run with different Γ, and a KS test confirmed (p-value $\gtrsim 0.9990$) the previous statement.

- $L_{\rm iso}$: The isotropically-equivalent luminosity determines the position of the photosphere ($R_{\rm ph}$) and thus the initial radius of the simulations, as well as the value of the observed specific flux. Since our results were peak-normalized in order to better compare the effect of other parameters, both of these factors bear no impact in the shape of the spectrum.

- $N_{\rm col}$: Figure 2.2 shows the results of simulations with different fraction of collected photons. We considered a range from 1/6 of the total number of photons to 5/6 of the total, in increments of 1/6. The results are remarkably similar and a KS test shows that there's no statistically significant difference between 1/6 and a 1/3 (p-value $\gtrsim 0.9999$), nor between 1/3 and 5/6 (p-value $\gtrsim 0.9999$). We consider 1/3 as an intermediate value that provides enough photons and physically representative results, without requiring additional runtime. In this sense, the obtained spectra are time-averaged and not instantaneous.

2.3 Comptonization of thermal photons with one dissipation event

2.3.1 Simulation results

Figure 2.3 shows a comparison between the three types of electron distributions in a similar way to that in Santana et al. (2015). Santana et al. (2015) make their comparison at three different photon temperatures and an optical depth of $\tau_{\rm initial} = 2$. Here we limit ourselves to two photon temperatures

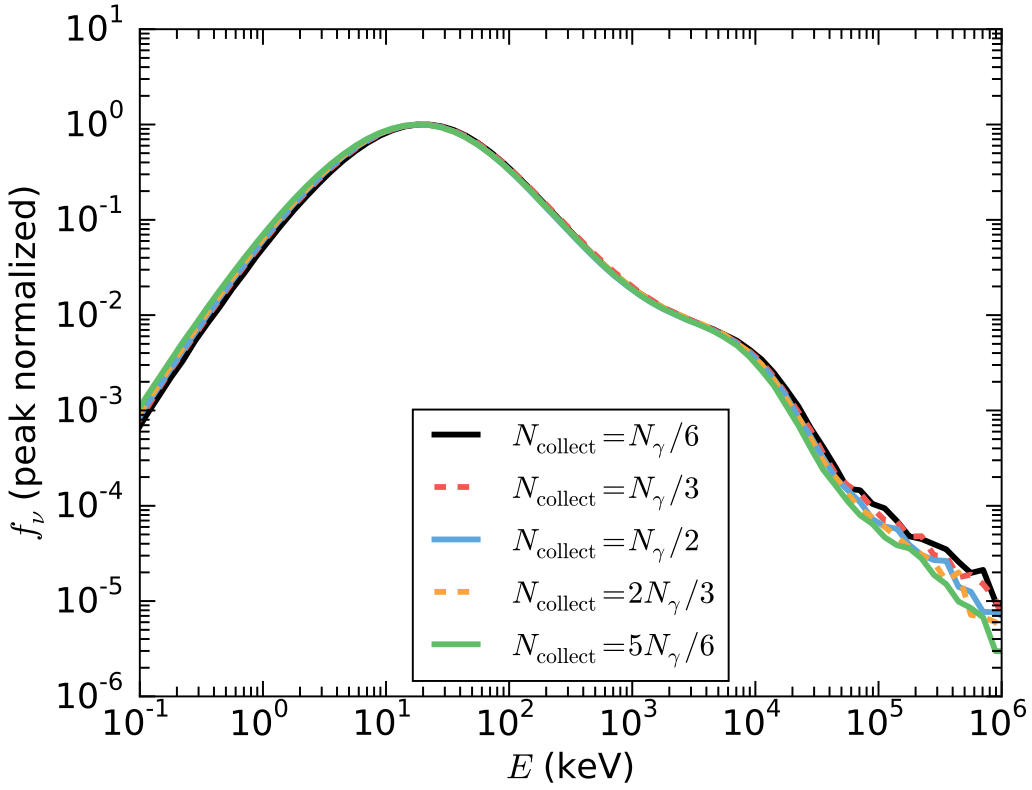

Figure 2.2: Effect of changing the fraction of collected photons. Here $\Gamma = 300$, $\tau_{\rm initial} = 5$, $k_B T'_\gamma = 30$ eV, MB electron distribution, and $k_B T'_e = (\gamma_{\rm elec}^{\rm AD} - 1)(80-1)m_e c^2$. Note the small discrepancy between all the cases.

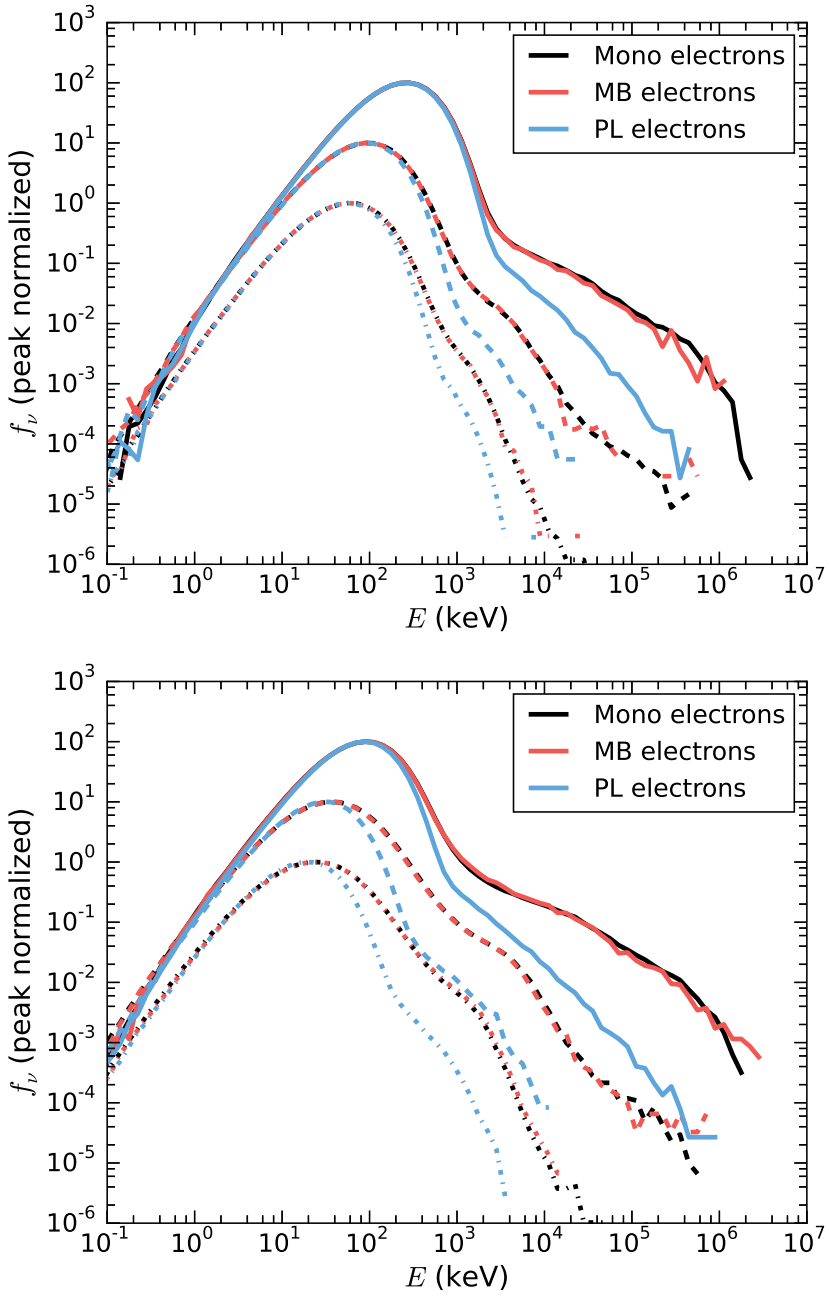

Figure 2.3: *Top panel:* Comparison between the three types of electron distributions at different optical depths. For all these runs, $k_B T'_\gamma = 300$ eV and $\gamma_e = 30$. The solid lines are for $\tau_{\rm initial} = 2$, the dashed for $\tau_{\rm initial} = 8$, and the dot-dashed for $\tau_{\rm initial} = 16$. *Bottom panel:* Same as *Top panel* but with $k_B T'_\gamma = 100$ eV and $\gamma_e = 50$.

(300 and 100 eV) but show additional comparisons at $\tau_{\rm initial} = 8$ and $\tau_{\rm initial} = 16$. For the case of $k_B T'_\gamma = 300$ eV, the mono-energetic electrons were set to $\gamma_e = 30$, the MB electrons to $k_B T'_e = (\gamma_{\rm elec}^{\rm AD} - 1)(30 - 1) m_e c^2$, and the PL electrons from $\gamma_{e,1} = 2$ to $\gamma_{e,2} = 30$ with an index of $p = 2.4$; whereas for the photon temperature of 100 eV the γ_e was changed in each expression to 50.

The results for both temperatures and all optical depths seem to be the same: MB and mono-energetic electrons tend to give very similar results, and they both seem better at generating a power law above the peak than PL electrons. The results with PL electrons present either a steep drop or a very steep power-law in all cases.

The similar results provided by MB and mono-energetic electrons makes sense: even though some electrons in the Maxwellian distribution will have values of $\gamma_e > 80$, most of them will have similar values of γ_e as that of the mono-energetic electrons; thus, the total energy budget of the electron population is comparable. That being said, we feel that a MB distribution is more likely to occur in nature than a mono-energetic and we will then run most of the simulations using this distribution.

The previous comparison is not entirely fair to the PL distribution, since in both cases the power-law was set to begin at $\gamma_{e,1} = 2$ and end at the higher $\gamma_{e,2}$ (either 30 or 50). The discrepancy is clear if we consider the average value of γ_e in a PL distribution:

$$\langle \gamma_e \rangle = \frac{\displaystyle\int_{\gamma_{e,1}}^{\gamma_{e,2}} \gamma_e \frac{dn_e}{d\gamma_e}\, {\rm d}\gamma_e}{\displaystyle\int_{\gamma_{e,1}}^{\gamma_{e,2}} \frac{dn_e}{d\gamma_e}\, {\rm d}\gamma_e} = \left(\frac{p-1}{p-2}\right) \left(\frac{\gamma_{e,1}^{-(p-2)} - \gamma_{e,2}^{-(p-2)}}{\gamma_{e,1}^{-(p-1)} - \gamma_{e,2}^{-(p-1)}}\right) \tag{2.4}$$

As long as $p \neq 2$. For $p = 2.4$, $\gamma_{e,1} = 2$, and $\gamma_{e,2} = 30$ Eq. (2.4) yields an average $\gamma_e \approx 4.7$, whereas a value of $\gamma_{e,2} = 80$ we find $\langle\gamma_e\rangle \approx 5.1$. Even if we consider the unphysical limit of $\gamma_{e,2} \to \infty$, $\gamma_{e,1}$ will approach the asymptotic value of

$$\lim_{\gamma_{e,2}\to\infty} \langle\gamma_e\rangle = \left(\frac{p-1}{p-2}\right)\gamma_{e,1} \tag{2.5}$$

As long as $p > 2$[2]. For $p = 2.4$ this limit is 7. This makes sense since for this value of p most of the electrons will lie close to $\gamma_{e,1}$. Thus, the electron population has on average less energy by a factor of ~ 10 compared to the mono-energetic and MB distributions. We then decided to run simulations with a PL *starting* at $\gamma_e = 80$ and extending to higher γ_e.

The results can be seen on Figure 2.4. Note that, in comparison with the $\tau_{\rm initial} = 2$ simulations of Figure 2.3, the dip above the peak is less pronounced; though still no power-law can be definitely seen. However, a comparison with a MB distribution with $k_B T'_e = (\gamma^{\rm AD}_{\rm elec} - 1)(80 - 1)m_e c^2$ shows that even with this increased value of $\gamma_{e,2}$, the MB distribution yields similar results for 3–4 decades above the peak, and only differs at the highest end.

On the other hand, perhaps the reason why the PL produces such results is that the index p of the distribution is too large (steep) and thus the electrons aren't getting enough energy on average. Figure 2.5 shows the results for different values of p. Notice that, in agreement with equation (2.4), as the value of p decreases the average γ_e increases hardening the spectrum. However, the average γ_e is still less than that for a MB distribution with $\gamma_e = 80$, and a

[2]If $p \leq 2$ the above limit is not valid and $\gamma_{e,2} \to \infty$. This is completely reasonable since the expression in eq. 2.4 is lower-bounded by $1/\gamma_e$ for $p < 2$, i.e., $\langle\gamma_e\rangle > 1/x$.

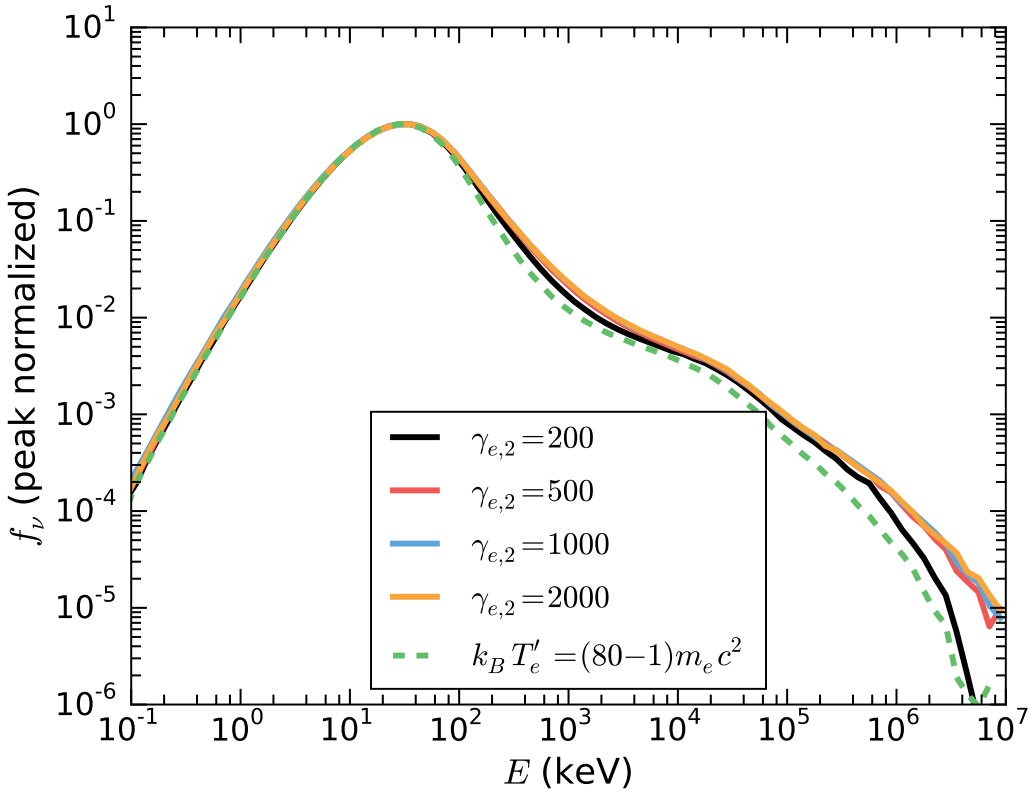

Figure 2.4: Comparison of different $\gamma_{e,2}$ for electron power-law distributions. Here we chose $k_B T'_\gamma = 30$ eV, $\gamma_{e,1} = 80$, $p = 2.4$, and $\tau_{\rm initial} = 2$. Also shown for reference are the simulation results with MB electrons and $k_B T'_e = (\gamma_{\rm elec}^{\rm AD} - 1)(80 - 1) m_e c^2$.

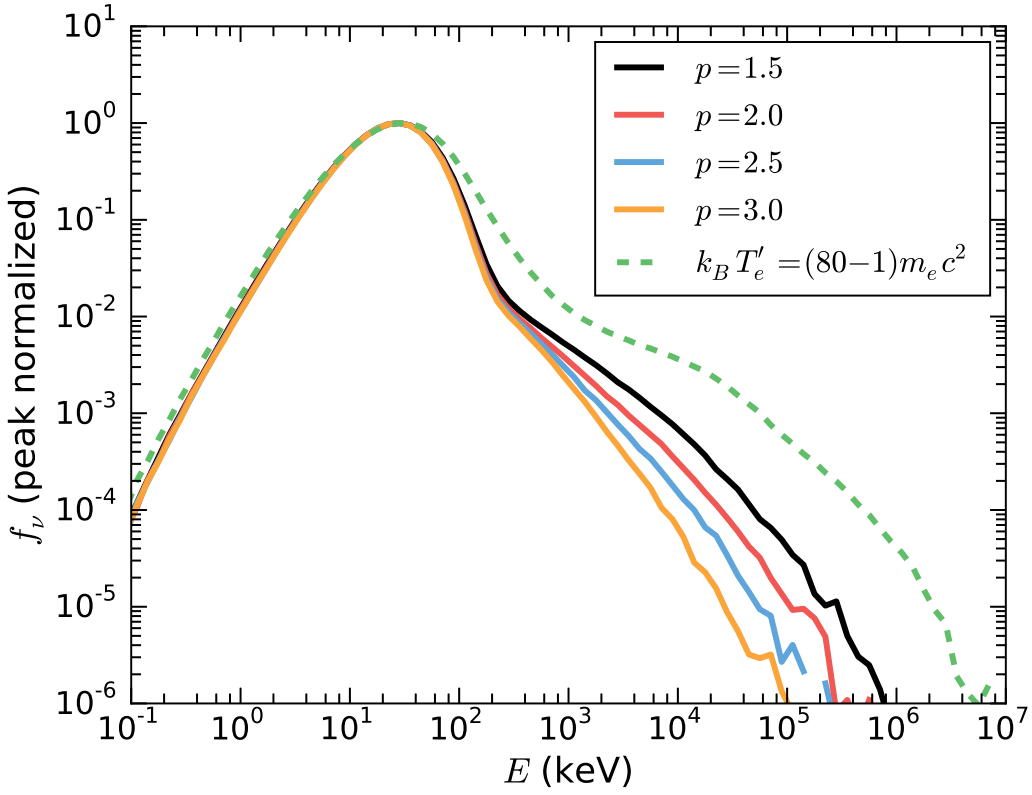

Figure 2.5: Comparison of different power-law indices p for electron power-law distributions. Here $\Gamma = 300$, $k_B T'_\gamma = 30$ eV, $\gamma_{e,1} = 2$, $\gamma_{e,2} = 80$, and $\tau_{\rm initial} = 2$. Just like in Fig. 2.4, we also show the results of a MB distribution with $k_B T'_e = (\gamma^{\rm AD}_{\rm elec} - 1)(80 - 1) m_e c^2$

significant dip after the peak energy is still present. This fortifies our decision to run mostly with a MB distribution.

Another parameter worth exploring is the seed photon temperature $k_B T'_\gamma$. Figure 2.6 shows the results of such simulations where we also have included the spectrum of the electrons (dashed lines) at the end of each simulation. In the top panel of Figure 2.6 we can observe that, as expected, a lower photon temperature will have the effect of shifting the whole spectrum

to lower energies, but the difference in the spectral features is not obvious. The lower panel shows the same results but with the x–axis normalized and the differences now become clear: the spectra with lower photon temperatures will have a higher flux at energies above the peak.

The effect of Adiabatic cooling is shown in Figure 2.7 for three different optical depths and two photon temperatures. Both panels are shown with a x–normalized axis, and the results show that there isn't a significant difference between the two of them, and the small discrepancies are only noticeable at higher optical depths. As expected, the flux at higher energies is slightly less for the case of AC, but IC clearly is the dominant cooling mechanism.

Summarizing, the results presented in this section are:

- The bulk LF and collected fraction of photons have no impact on the spectrum.
- AC will decrease the peak energy of the spectrum for $\tau_{\rm initial} \gtrsim$ a few, but it has a less significant impact on the shape of the spectrum.
- Both MB and mono-energetic distributions will provide better results than a PL distribution.
- Most of the simulations present a dip of 2–3 orders of magnitude right above the peak energy, in contrast with the expected peak–then–power-law behavior.
- Lower photon temperatures will populate parts of the spectrum above the peak energy more than higher photon temperatures.

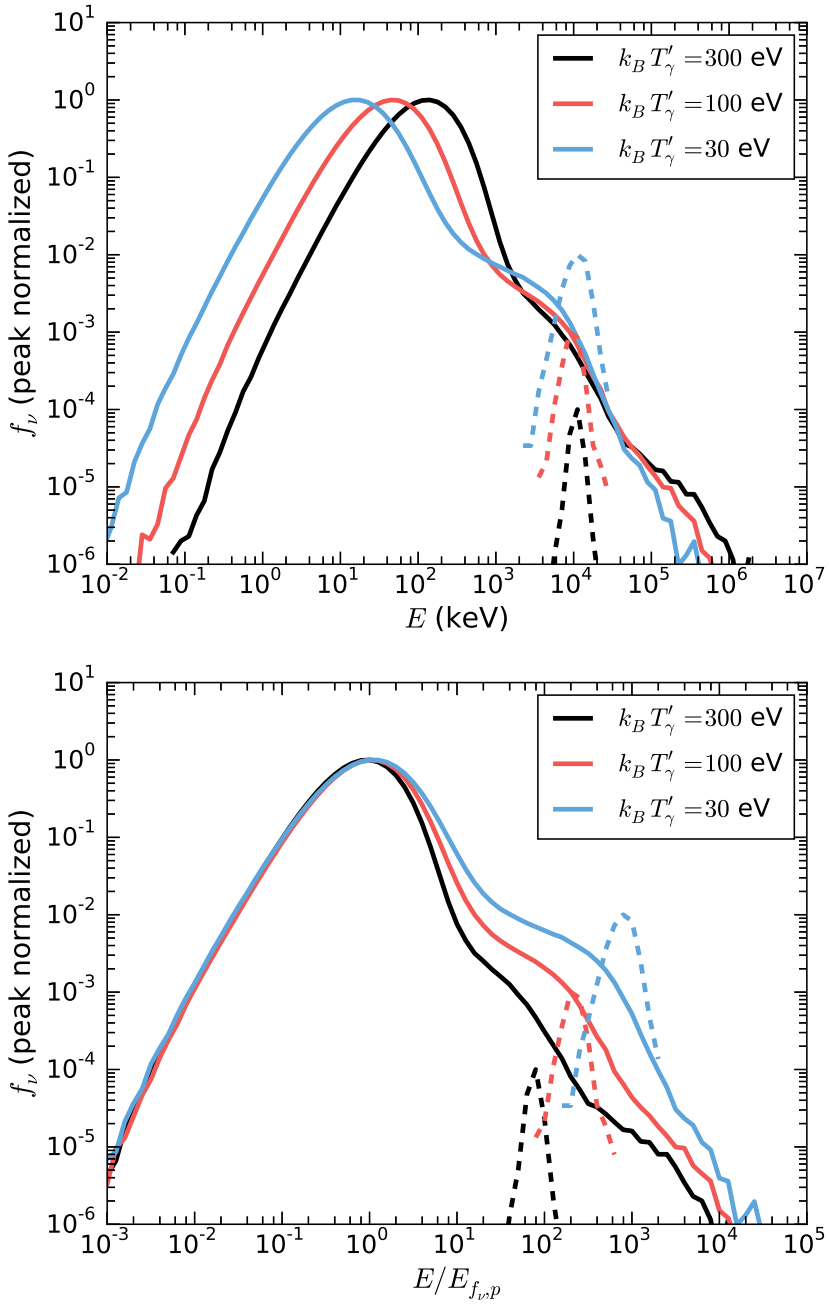

Figure 2.6: *Top panel:* Comparison of different seed co-moving photon temperatures. All runs were done with a MB electron distribution with $\Gamma = 300$, $k_B T'_e = (\gamma_{\rm elec}^{\rm AD} - 1)(30-1)m_e c^2$ and $\tau_{\rm initial} = 5$. *Bottom panel:* Same as *Top panel* but with the $x-$axis normalized so that $f_\nu(x=1) = 1$. In both cases, the dashed lines represent the electrons at the end of the simulations.

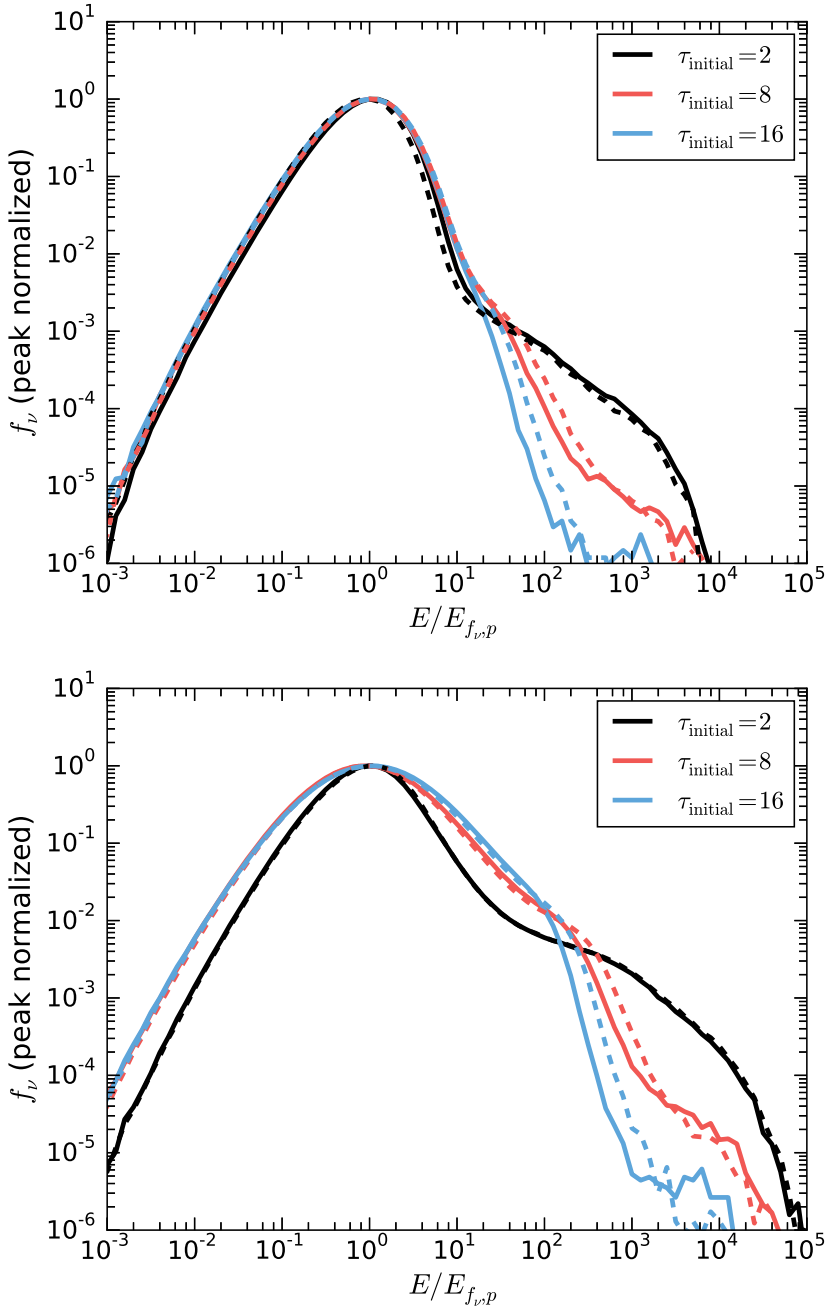

Figure 2.7: *Top panel:* Comparison of simulations run with and without Adiabatic Cooling (AC) at different $\tau_{\rm initial}$. In all cases we chose a mono-energetic distribution with $k_B T'_\gamma = 300$ eV and $\gamma_e = 30$. The solid lines are with AC turned off and the dashed ones with AC on. *Bottom panel:* Same as *Top panel* but with $k_B T'_\gamma = 30$ eV and $\gamma_e = 80$.

2.3.2 Discussion of the results

The last two points presented in section (2.3) are perhaps the most new and surprising. Until now, previous works had shown the expected peak–then–power-law behavior that's in more agreement with the observed Band function. As we will see, the two of them are connected and we will try to understand and explain them. Our intention is to present an analytical estimate without going through the details of a rigorous derivation, referring the reader to Santana et al. (2015) for more details.

It is possible to estimate the condition required to produce a power-law above the peak as

$$N_{\rm Comp} \gtrsim \frac{N_\gamma}{N_e} \approx 10^5 \tag{2.6}$$

Here, $N_{\rm Comp}$ is the number of scatterings it takes to cool an electron from its initial LF to a critical value where Comptonization stops being effective, $\gamma_{e,\rm Comp}$. Eq. (2.6) tells us that this number has to be bigger than the ratio of photons to electrons, otherwise a sizable fraction of the photons will remain very close to the peak.

To estimate $N_{\rm Comp}$ we start with the definition of the Compton$-Y$ parameter (Rybicki & Lightman, 1986):

$$Y = 2\tau_{\rm initial} \cdot \max\left[\frac{4k_B T'_e}{m_e c^2}, \frac{4}{3}(\gamma_e^2 - 1)\right] \tag{2.7}$$

Since Compton$-Y \geq 1$ in order for Comptonization to be effective, this expression allows us to calculate $\gamma_{e,\rm Comp}$ as $\gamma_{e,\rm Comp} = 1 + 1/8\tau_{\rm initial}$, so that $\gamma_{e,\rm Comp} = 1.06$ and 1.008 for $\tau_{\rm initial} = 2$ and 16, respectively. With this, we can

$\tau_{\rm initial} = 2$	$N_{\rm Comp,MR}$	$N_{\rm Comp,rel}$
$k_B T'_\gamma = 30$ eV	~ 4200	$\sim 7000\,(\gamma_{e,i} = 80)$
$k_B T'_\gamma = 100$ eV	~ 1300	$\sim 2000\,(\gamma_{e,i} = 50)$
$k_B T'_\gamma = 300$ eV	~ 420	$\sim 700\,(\gamma_{e,i} = 30)$
$\tau_{\rm initial} = 16$	$N_{\rm Comp,MR}$	$N_{\rm Comp,rel}$
$k_B T'_\gamma = 30$ eV	~ 7400	$\sim 10^4\,(\gamma_{e,i} = 80)$
$k_B T'_\gamma = 100$ eV	~ 2200	$\sim 3000\,(\gamma_{e,i} = 50)$
$k_B T'_\gamma = 300$ eV	~ 740	$\sim 1000\,(\gamma_{e,i} = 30)$

Table 2.1: Values of $N_{\rm Comp}$ for the parameters considered in this work for optical depths of 2 and 16. The values for $\tau_{\rm initial} = 8$ can be interpolated from the ones presented here.

find an expression for the number of scatterings it takes an electron to cool from $\gamma_{e,i}$ to $\gamma_{e,\rm MR} \equiv 2$, and from $\gamma_{e,\rm MR} = 2$ to $\gamma_{e,\rm Comp}$. Denoting the first one as $N_{\rm cool,rel}$ and the second one as $N_{\rm cool,MR}$, we have Santana et al. (2015, eqs. (23) and (24))

$$N_{\rm cool,rel} = \frac{3 m_e c^2}{8 E'_\gamma} \ln\left[\frac{(\gamma_{e,\rm MR}+1)(\gamma_{e,i}-1)}{(\gamma_{e,\rm MR}-1)(\gamma_{e,i}+1)}\right] \tag{2.8}$$

$$N_{\rm cool,MR} = \frac{m_e c^2}{4 E'_\gamma} \ln\left[\frac{\gamma_{e,i}-1}{\gamma_{e,\rm Comp}-1}\right] \tag{2.9}$$

Where we are making the approximation $E'_\gamma \approx 2.8 k_B T'_\gamma$, which is not a bad one considering most of the photons lie near the peak of the BB spectrum. The first equation is valid for $\gamma_{e,i} > 2$ and the second for $\gamma_{e,i} \leq 2$. In the first case, $N_{\rm Comp,rel} = N_{\rm cool,rel} + N_{\rm cool,MR}$, whereas for the latter $N_{\rm Comp,MR} = N_{\rm cool,MR}$. Table 2.1 summarizes the values of $N_{\rm Comp}$ for our main parameters.

This clearly shows that at lower photon temperatures more scatterings are required to cool-down an electron, or equivalently, that lower photon temperatures allow Compton$-Y$ to stay above 1 for longer time, meaning electrons can 'pump' up more photons to energies above the peak.

Notice that, for the cases of $k_B T'_\gamma = 100$ and 300 eV, $N_{\rm Comp} \ll 10^5 = N_\gamma/N_e$. In particular, for a temperature of 300 eV we see that $\frac{N_{\rm Comp}}{N_\gamma/N_e} \sim 10^{-4}$, which is about an order of magnitude larger than the dip observed in the top panel of Figure 2.3. On the other hand for $k_B T'_\gamma = 100$ eV, $\frac{N_{\rm Comp}}{N_\gamma/N_e} \sim 30$ for a $\tau_{\rm initial} = 16$. This result seems to disagree with the existence of a short power-law above the peak for this simulation. There are two factors that satisfactorily reconcile this discrepancy:

1. The analytical estimate presented above ignores one critical but important fact: that, at some point after the electrons have lost most of their energy, there is the possibility they'll encounter a photon with higher energy and undergo Compton scattering, partially reheating the electron. Figure 2.8 shows the γ_e history of three electrons from one of our simulations. Notice that after steadily decreasing, the electrons experience a few episodes where their γ_e goes back up to ~ 5. There are at least ~ 10 episodes where it increases to $\gamma_e = 2$. Since $N_{\rm Comp} \sim 2500$ for a γ_e of 5 and $k_B T'_\gamma = 100$ eV, this could increase the effective number of scatterings in $N_{\rm Comp}$ by a factor of 10.

2. We've performed approximations of order unity in some terms, for example, approximating the number of photons in the peak as the total number of photons, that is, $E'_\gamma \sim E_{\rm peak}$. These can add up to a factor of $\sim 3 - 5$.

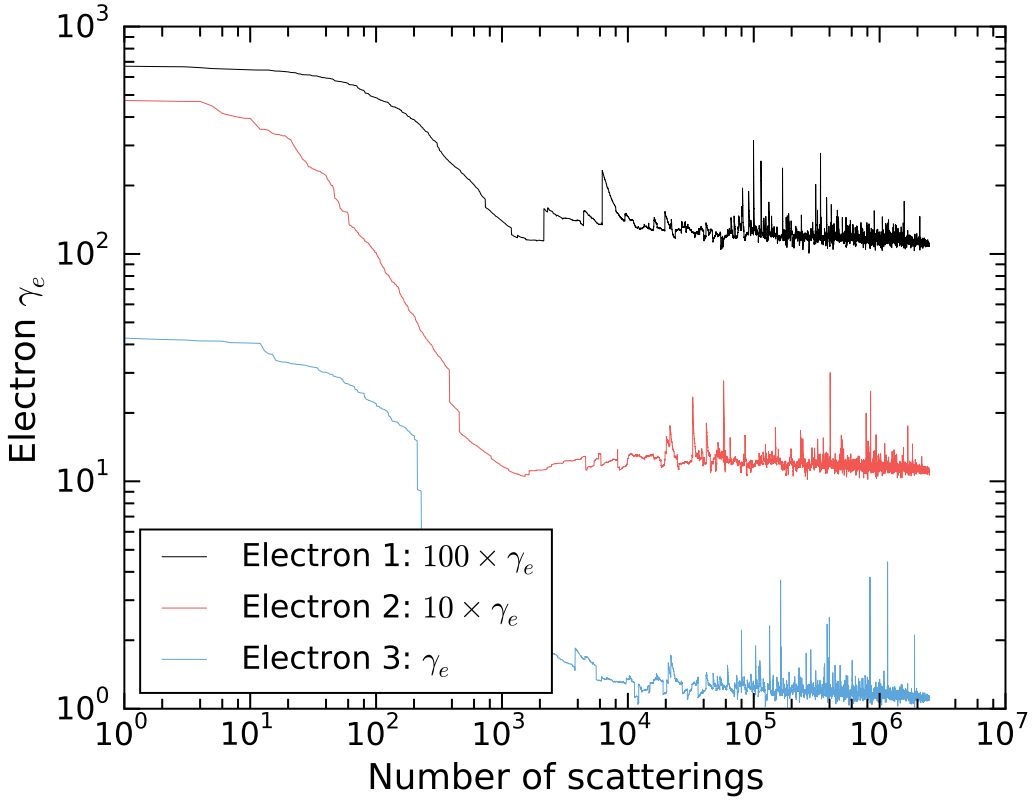

Figure 2.8: Evolution of γ_e as a function of the number of scatterings. Shown are three electrons from the MB distribution simulation with $\tau_{\text{initial}} = 8$ of Figure 2.2.

These two factors combined can satisfactorily explain the discrepancy in our estimations, thus providing us a clearer picture of the physical reasons for the presence of the dip above the peak, as well as the requirements to form a power-law above it.

2.4 Comptonization of thermal photons with reheating events

2.4.1 Simulation results

Figure 2.9 shows the results of reheating the electrons on multiple occasions to the same LF as the initial one. We show the effect for two different photon temperatures and different values of γ_e. The result is the same as we increase the number of reheating events for both cases: a progression from a dip above the peak with no power-law, to the expected peak–then–power-law, to a deformed or modified spectrum that deviates from it.

Figure 2.10 shows the results of a different reheating scheme. Here the total amount of energy to be dissipated is kept constant at a value of $k_B T'_e = (\gamma_{\rm elec}^{\rm AD} - 1)(50 - 1)m_e c^2$, and it is evenly distributed amongst the total number of dissipation events (number of reheating events plus one). The trend here is that, as the number of reheating events increases, the flux at the highest energies decreases while the one a couple of decades above the peak increases. The dip present for $N_{\rm reheat} = 0$ becomes a power-law by $N_{\rm reheat} = 30$.

Figure 2.11 shows the result of changing the region over which the reheating events take place by varying the 'spread fraction' parameter explained at the end of Section 2.1. We considered different cases ranging from a spread of 1 (which corresponds to the reheating events taking place between $\tau = 10$ and $\tau = 1$) to a spread 1/4 (which corresponds to the reheating events taking place between $\tau = 10$ and $\tau = 7.5$). The spectra are very similar showing only smaller differences at the high-end. The general trend is that, as the reheating gets spread over a broader range of optical depths (i.e. a larger spread fraction), the flux slightly increases at higher energies.

Summarizing, the results presented in this section are:

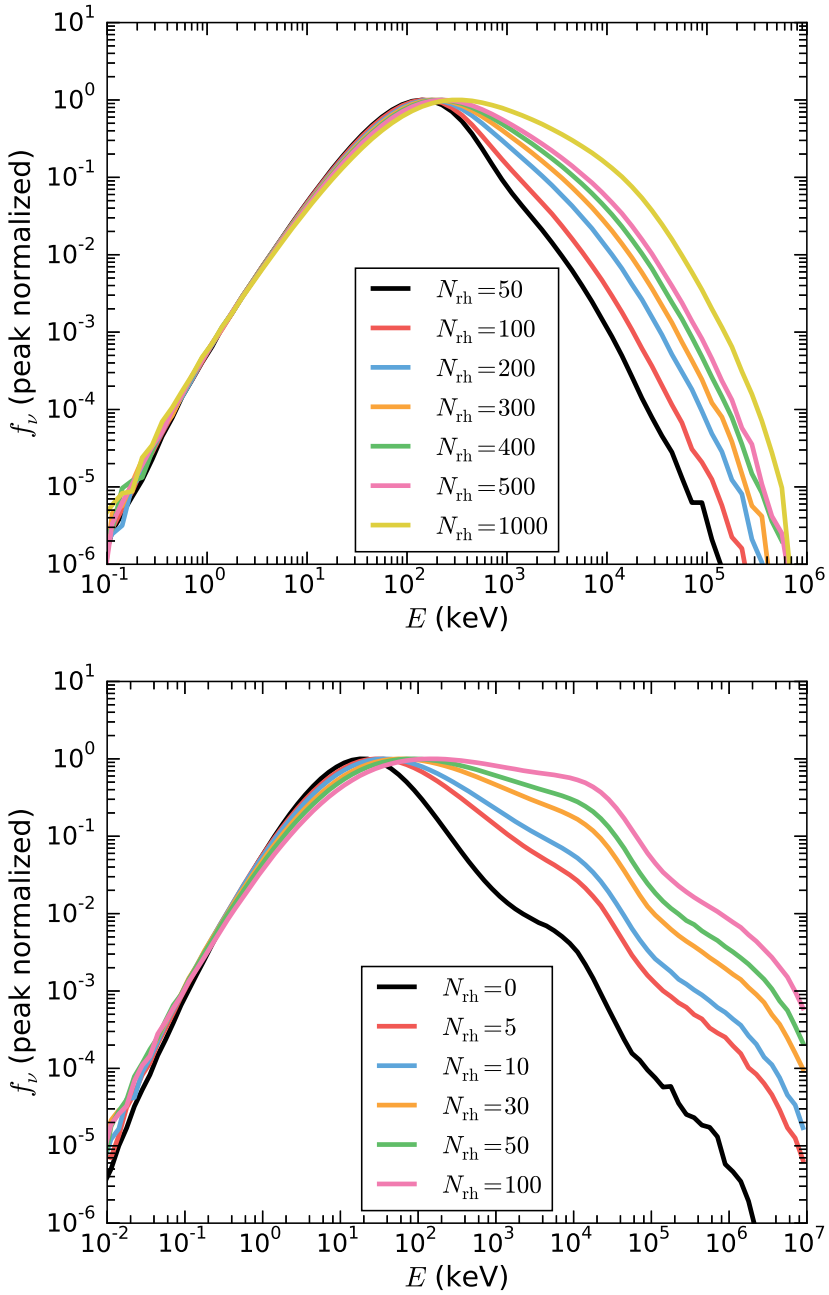

Figure 2.9: *Top panel:* Effect of different number of reheating events for a MB distribution with $\Gamma = 300$, $k_B T'_\gamma = 300$ eV and $\tau_{\rm initial} = 5$. In every reheating event the electrons are heated back to their initial temperature of $k_B T'_e = (\gamma^{\rm AD}_{\rm elec} - 1)(2-1)m_e c^2$. *Bottom panel:* Same as *Top panel* but with $k_B T'_\gamma = 30$ eV and $k_B T'_e = (\gamma^{\rm AD}_{\rm elec} - 1)(80-1)m_e c^2$.

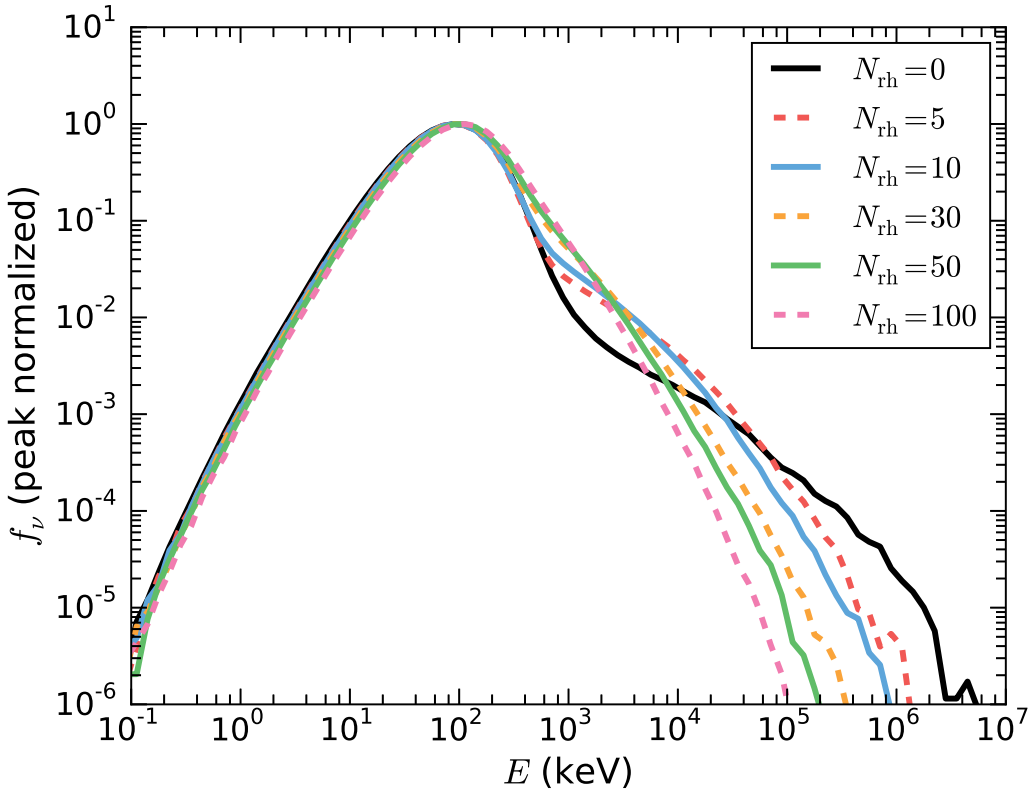

Figure 2.10: Results for the constant-energy dissipation scheme discussed in Section (2.4). The simulations were run with $\Gamma = 300$, $k_B T'_\gamma = 100$ eV, $k_B T'_{e,\rm total} = (\gamma^{\rm AD}_{\rm elec} - 1)(50 - 1)m_e c^2$, and $\tau_{\rm initial} = 5$.

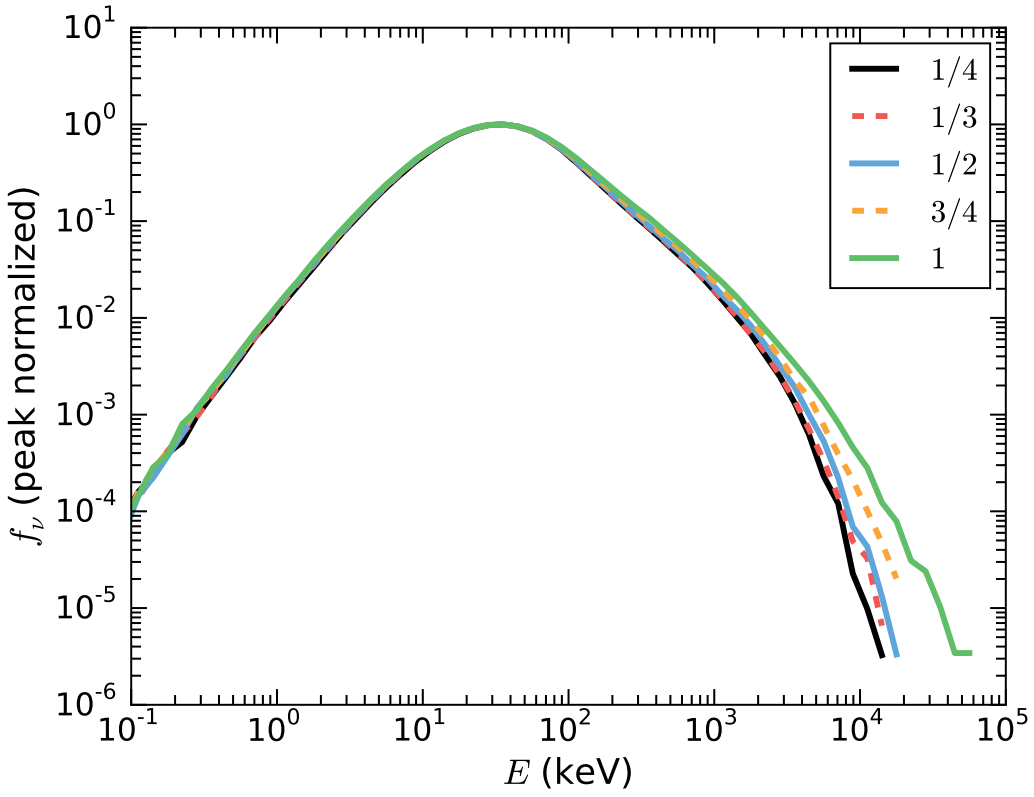

Figure 2.11: Results for the uneven dissipation scheme discussed in Section (2.4). The simulations were run with $\Gamma = 300$, $k_B T'_\gamma = 100$ eV, $k_B T'_{e,\mathrm{total}} = (\gamma^{\mathrm{AD}}_{\mathrm{elec}} - 1)(50 - 1) m_e c^2$, and $\tau_{\mathrm{initial}} = 10$.

- There is a critical number of reheating events that will yield a power-law. Less events and a dip is still present, more events and the spectrum deviates from the expected power-law.
- Given a fixed total dissipation energy, more reheating events will better populate the energies above the peak at the expense of losing photons from the high-energy tail.
- Reheating gives the best results when it's spread between the whole interval starting at τ_{initial} and ending $\tau_{\text{photosphere}}$.

2.4.2 Discussion of the results

The first point of the previous summary indicates us that we have two important number of reheating events: $N_{\text{reheat,min}}$ and $N_{\text{rh,max}}$. The first one is the number required to generate a power-law, while the second is the number at which the spectrum deviates from a power-law. A simple analysis reveals we can estimate $N_{\text{reheat,min}}$ as

$$N_{\text{reheat,min}} = \frac{N_\gamma / N_e}{N_{\text{Comp}}} \tag{2.10}$$

For the case pictured in the top panel of Figure 2.9, we find that $N_{\text{reheat,min}} = 10^5/450 \sim 225$ and our results seem to agree with that: a good power-law can be observed for both 200 and 300 reheating events. Similarly, for the bottom panel we have $N_{\text{reheat,min}} = 10^5/10^4 \sim 10$. Notice that for 5 and 10 reheating events there is a short power-law above the peak, though it is followed by a dip at an energy $\sim 10^5$ keV.

On the other hand, we propose a simple estimate for the maximum number of reheating events: $N_{\text{reheat,max}} = 10 N_{\text{reheat,min}}$. This estimate is moti-

vated by the fact that at this point the electrons probably don't have enough time to cool-off between dissipation events, resulting in a large fraction of photons being scattered by electrons with large values of γ_e[3]. Both of our plots are consistent with this estimate: for the top panel the spectrum shows significant curvature by $N_{\rm reheat} = 1000$, while in the bottom panel the spectrum has flattened out and warped by $N_{\rm reheat} = 50$.

These results also suggest that, in order to produce a power-law above the peak, a situation where small a amount of energy is dissipated many times is preferred over one where more energy is released less frequently – notice that the total energy budget of the top panel of Figure 2.9 is only a factor of ~ 8 smaller than the bottom panel, but the results are quite different.

Finally, this last statement is also in agreement with both of our results from Figures 2.10 and 2.11, since the cases where the energy is distributed the most and more evenly provide the results.

2.5 Conclusions

The results provided by our code for a previously unexplored region of the parameter space soundly show the presence of a previously unobserved feature: a significant dip in the flux above the peak energy when the photon to electron ratio is a more realistic value of $\sim 10^5$. This drop is present in several of the simulations with different parameters, and an analytical estimate reinforces our confidence in the physical existence of this feature.

Additionally, we explore the dependence of the spectrum on several

[3]Recall that in the case of relativistic electrons, the change in photon energy is proportional to γ_e^2 (Rybicki & Lightman, 1986)

parameters in order to understand which ones have a bigger influence in modifying it from its initial Planckian shape. We found that bulk Lorentz factor and collected fraction of photons don't have a significant impact on the shape of the spectrum. Adiabatic cooling decreases the peak energy of the spectrum but only has a minimal effect in the shape of it. We also observed an equivalence between MB and mono-energetic electron distributions, both preferable over a power-law electron distribution.

The two factors with the greatest impact are the seed photon temperature and electron Lorentz factor. Lower photon temperatures are favorable since they tend to cool-off the electrons at a slower rate, i.e., more scatterings are needed, though this becomes an issue when trying to match the peak energy of the spectrum with the observed clustering of values around $200 - 300$ keV. Higher values of γ_e increase the energy budget of the electron population, allowing them to pump-up more photons above the peak.

Moreover, even though there are ways to obtain a spectrum more in line with the observed Band function, they appear to require some fine-tuning. In the specific case of reheating the allowed parameter space is narrow, and it is not clear what kind of mechanism could provide the required conditions.

It should be stated that these conclusions don't completely rule out the Photospheric process as a candidate for the radiation mechanism responsible for the GRB prompt emission; however, they do pose a serious challenge for its validity, and further study is required before reaching more definitive conclusions.

There are several avenues where the work presented here could be improved and further developed. For example, more realistic models for the dissipation mechanism could be considered instead of the ad-hoc ones employed

here, examples being – but not limited to – Coulomb scattering between protons and electrons or magnetic reconnection models for Poynting-dominated jets. Additionally, geometric effects could also be incorporated into the code with the possibility of broadening and flattening the spectrum below the peak, in an attempt to solve the problem of the low-energy index.

Another interesting idea is to develop more self-consistent models, for example, one could envision a scenario where a dissipation mechanism heats up electrons which then radiate a fraction of their energy through synchrotron or some other radiative mechanism. The outgoing spectrum would then be a superposition of Comptonized photons (thermal and non-thermal) and non-thermal radiation that escapes without being processed.

Bibliography

Band D. et al., 1993, ApJ, 413, 281

Bégué D., Iyyani S., 2014, ApJ, 792, 42

Bégué D., Siutsou I. A., Vereshchagin G. V., 2013, ApJ, 767, 139

Beloborodov A. M., 2010, MNRAS, 407, 1033

Briggs M. S. et al., 1999, ApJ, 524, 82

Chhotray A., Lazzati D., 2015, ApJ, 802, 132

Daigne F., Bošnjak Ž., Dubus G., 2011, A&A, 526, A110

Fishman G. J., Meegan C. A., 1995, ARA&A, 33, 415

Ghisellini G., Celotti A., 1999, A&AS, 138, 527

Goldstein A. et al., 2012, ApJS, 199, 19

Goodman J., 1986, ApJ, 308, L47

Ito H., Nagataki S., Matsumoto J., Lee S. H., Tolstov A., Mao J., Dainotti M., Mizuta A., 2014, ApJ, 789, 159

Kompaneets A. S., 1956, Zhurnal Eksperimental'noi i Teoreticheskoi Fiziki, 31, 876

Kouveliotou C., Meegan C. A., Fishman G. J., Bhat N. P., Briggs M. S., Koshut T. M., Paciesas W. S., Pendleton G. N., 1993, ApJ, 413, L101

Kumar P., Zhang B., 2015, Phys. Rep., 561, 1

Lazzati D., Begelman M. C., 2010, ApJ, 725, 1137

Lazzati D., Morsony B. J., Margutti R., Begelman M. C., 2013, ApJ, 765, 103

Liang E., Zhang B., Virgili F., Dai Z. G., 2007, ApJ, 662, 1111

Liang E. W., Yi S. X., Zhang J., L H. J., Zhang B. B., Zhang B., 2010, ApJ, 725, 2209

Longair M. S., 2011, High Energy Astrophysics

Lundman C., Pe'er A., Ryde F., 2013, MNRAS, 428, 2430

Melia F., 2009, High-Energy Astrophysics

Mészáros P., Rees M. J., 2000, ApJ, 530, 292

Molinari E. et al., 2007, A&A, 469, L13

Paczynski B., 1986, ApJ, 308, L43

Panaitescu A., Kumar P., 2001, ApJ, 560, L49

Panaitescu A., Kumar P., 2002, ApJ, 571, 779

Pathria R., Beale P., 2011, Statistical Mechanics. Elsevier Science

Pe'er A., Ryde F., 2011, ApJ, 732, 49

Piran T., 2004, Reviews of Modern Physics, 76, 1143

Preece R. D., Briggs M. S., Mallozzi R. S., Pendleton G. N., Paciesas W. S., Band D. L., 1998, ApJ, 506, L23

Preece R. D., Briggs M. S., Mallozzi R. S., Pendleton G. N., Paciesas W. S., Band D. L., 2000, ApJS, 126, 19

Rybicki G. B., Lightman A. P., 1986, Radiative Processes in Astrophysics

Santana R., Hernández R. A., Crumley P., Kumar P., 2015, MNRAS, submitted.

Sari R., Piran T., Narayan R., 1998, ApJ, 497, L17

Vereshchagin G. V., 2014, International Journal of Modern Physics D, 23, 1430003

Wanderman D., Piran T., 2010, MNRAS, 406, 1944

Xue, R.-R., Fan, Y.-Z., Wei, D.-M., 2009, A&A, 498, 671

Yost S. A., Harrison F. A., Sari R., Frail D. A., 2003, ApJ, 597, 459

Zhang B., Yan H., 2011, ApJ, 726, 90